TM LDH Meets Birnessite: A 2D-2D Hybrid Catalyst with Long-term Stability for Water Oxidation at Industrial Operating Conditions

Zhuwen Chen[a‡], Min Ju[a‡], Mingzi Sun[b], Li Jin[c], Rongming Cai[a], Zheng Wang[a], Lei Dong[a], Luming Peng[c], Xia Long[a*], Bolong Huang[b*], Shihe Yang[a*]

a. Guangdong Provincial Key Lab of Nano-Micro Material Research, School of Chemical Biology and Biotechnology, Shenzhen Graduate School, Peking University, Shenzhen, China.

b. Department of Applied Biology and Chemical Technology, The Hong Kong Polytechnic University, Hung Hom, Kowloon, Hong Kong SAR, China.

c. Key Laboratory of Mesoscopic Chemistry of MOE and Collaborative Innovation Center of Chemistry for Life Sciences, School of Chemistry and Chemical Engineering, Nanjing University, 163 Xianlin Road, Nanjing 210023, China.

ABSTRACT: Efficient noble-metal free electrocatalyst for oxygen evolution reaction (OER) is critical for large-scale hydrogen production via water splitting. Inspired by Nature's oxygen evolution cluster in photosystem II and the highly efficient artificial OER catalyst of NiFe layered double hydroxide (LDH), we designed an electrostatic 2D-2D assembly route and successfully synthesized a 2D LDH(+)-Birnessite(-) hybrid. The as-constructed LDH(+)-Binessite(-) hybrid catalyst showed advanced catalytic activity and excellent stability towards OER under a close to industrial hydrogen production condition (85 ºC and 6 M KOH) for more than 20 h at the current densities larger than 100 mA/cm². Experimentally, we found that besides the enlarged interlayer distance, the flexible interlayer NiFe LDH(+) also modulates the electronic structure of layered MnO_2, and creates an electric field between NiFe LDH(+) and Birnessite(-), wherein OER occurs with a greatly decreased overpotential. DFT calculations confirmed the interlayer LDH modulations of the OER process are attributable to the distinct electronic distributions and environments. Upshifting the Fe-3d orbitals in LDH promotes electron transfer from the layered MnO_2 to LDH, significantly boosting up the OER performance. This work opens a new way to fabricating highly efficient OER catalyst for industrial water oxidation.

Introduction

Advanced catalysts for oxygen evolution reaction (OER) are the key for efficient water-splitting based hydrogen production.[1,2] Among the noble-metal free electrocatalysts of OER reported to date, NiFe LDH showed the best catalytic activity,[3-5] making it one of the most promising catalysts for industrial applications, but its stability need to be further improved. Meanwhile, Birnessite (**Scheme 1A&1B**), having a local atomic structure similar to oxygen evolution complex (OEC, **Scheme 1C**)[6] in photosystem II (PS II), also has been widely investigated. However, despite its tantalizing prospect as a mimic of OEC, birnessite exhibits a performance far below satisfactory. Many studies have been reported to investigate and enhance the activity of birnessite by modifying its internal and external structural features.[7-10] For example, trivalent metal ions such as Mn^{3+} and Co^{3+} have been incorporated into the MnO_2 layer by substitution, which indeed enhanced the water oxidation activity of birnessite due to the favourably tuned band structure.[11-16] Another strategy that has been applied was the modification of the interlayer cations.[13,15,17-20] By intercalating various alkali and alkaline earth cations into the interlayers, Kurz and co-workers found a correlation between the interlayer cation and the activity of birnessite, and Ca^{2+} and Sr^{2+} intercalated birnessites were found to be much more efficient catalysts towards OER in the presence of chemical oxidants than other cations intercalated birnessites.[21] However, the fundamental reasons behind this observation are still unclear at present.

Recently, a computational work[12] revealed that the interlayer cations of birnessite has a pronounced effect on the overall electronic structure, more like a ligand effect rather than directly bonding to oxygen to form a cubane-like structure as in OEC.[6] Calculations showed changes in band structure and density of states when these cations were varied. However, the exact role of intercalated ions in the catalytic performance of birnessite is still inconclusive. Anyway, the existence of Mn (III) doesn't tell the whole story about the catalytic activity of birnessite, and one also need consider chemical composition such as the above mentioned interlayer cations, as well as crystal phase, morphology, to name but a few.[22]

It is thought provoking to combine the common two-dimensional (2D) layered structure of the highly active but stability lacking NiFe LDH and the fairly stable but activity lacking birnessite, and more interestingly, their complementary charges, positive and negative, respectively. With a view to creating synergistic features of the two layered materials and getting the best of the two worlds, we successfully fabricated a NiFe LDH(+) intercalated birnessite(-) hybrid catalyst (labelled as LDH-Bir). The positively charged monolayer LDH acted

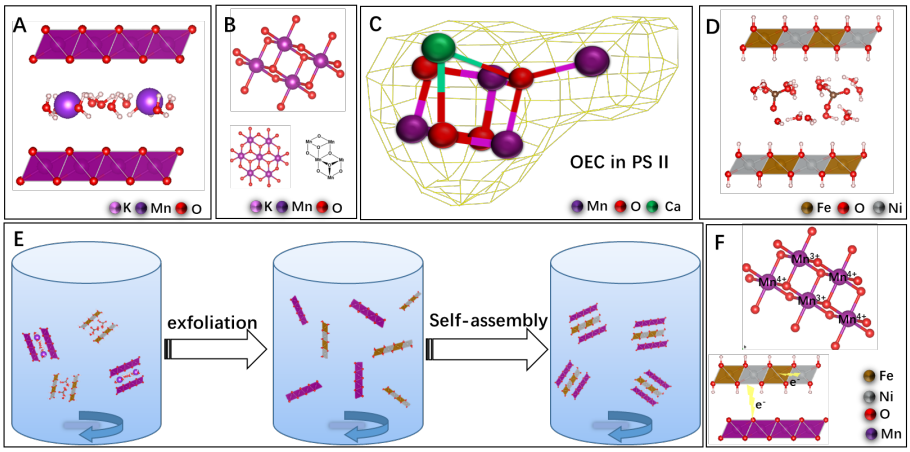

Scheme 1. Schematic illustrating the atomic structure of (A-B) Birnessite, (C) oxygen evolution cluster (OEC) in photosystem II, and (D) NiFe LDH, (E) fabrication of LDH(+)-Bir(-) hybrid by exfoliation and electrostatic self-assembly processes, (F) Mn(III) dispersed and stabilized in MnO_2 matrix (top) and the electron transfer between the Ni, Fe and Mn ions in the LDH(+)-Bir(-) hybrid catalyst (bottom).

as the charge compensating cations between the negatively charged octahedral MnO_2 layers of birnessite. More importantly, the structure and OER performance of the LDH(+)-Bir(-) hybrid catalyst were systematically investigated both experimentally and theoretically. Conceivably, the enlarged interlayer distance would facilitate the fast mass transport in between, and the flexible electronic structure of the interlayer NiFe LDH would modulate the electronic environment of the layered MnO_2, viz., create an electric field between the two due to their opposite charges. These distinct features have allowed to greatly improve the catalytic activity and stability of the hybrid catalyst at the same time even under the industrial hydrogen production conditions. Moreover, our theoretical calculations suggest that the LDH(+)-Bir(-) harbors an optimal electronic environment with a perfect linear correlation to electron transfer between the two oppositely charged layers, which guarantees both high activity and long stability towards OER.

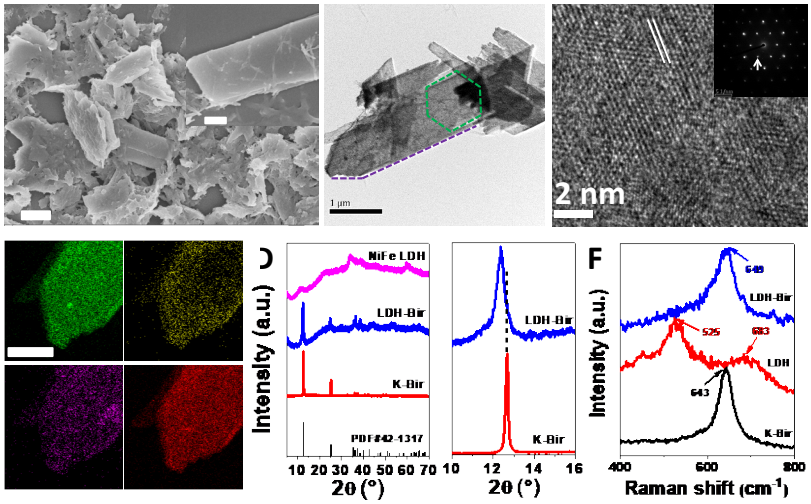

Figure 1. Morphology and structure characterizations of the as-prepared birnessites. (A) SEM images, (B) Elemental mapping images, (C) TEM image, (D) XRD patterns (left panel: XRD at the whole range, right panel: enlarged XRD pattern at ~12.5 º, (E) high resolution TEM (HRTEM) and ED pattern, (F) Raman spectra of LDH-Bir. The peak at ~643 cm^{-1} is due to the Raman mode of birnessite, while the Raman mode of LDH is at ~ 525 cm^{-1}.

Results

Both the birnessite (**Scheme 1A**) and LDH (**Scheme 1D**) samples exhibited a two-dimensional (2D) microstructure, and thus could be exfoliated to negatively charged $[Mn(III/VI)O_2]^{y-}$ and positively charged $[NiFe(OH)_2]^{x+}$ monolayers, respectively, in free-standing form. The complementary charges of the 2D materials allowed us to fabricate the LDH(+)-Bir(-) hybrid via electrostatic interaction between the exfoliated NiFe LDH layers and the exfoliated birnessite layers (Scheme 1E).

The scanning electron microscopy (SEM) images (**Figure 1A&S1**) clearly show that the as-prepared LDH(+)-Bir(-) hybrid maintained the same two-dimensional (2D) microsheet structures as the original K-Bir (**Figure S2**) with a uniform distribution of Mn, Ni, Fe and O elements (**Figure 1B, Figure S3**), but the lateral sizes of LDH-Bir were much larger than the pristine NiFe LDH nanosheets (**Figure S4**). Moreover, from the TEM image (**Figure 1C**), the 2D structure of the hybrid catalyst was further confirmed. And the XRD patterns (Figure 1B, PDF#42-1317) verified the retention of the crystal phases of Δ-MnO_2 for the LDH-Bir. However, due to the different sizes of monolayer LDHs and K ions, the hybridization increased the interlayer distance to 0.716 nm (LDH-Bir) from 0.698 nm (K-Bir), according to the diffraction peaks at 12.67 º (**Figure 1D**, right panel). The high resolution TEM (HRTEM) image (**Figure 1E**) and the corresponding ED pattern (**Figure 1E**, inset) also showed an interlayer expansion of the birnessite due to the intercalation of LDH monolayer (**Figure S5**).

Raman scattering spectroscopy is sensitive to the short-range order of materials, and was also employed to investigate the short-range atomic structure of the LDH-Bir hybrid. As we know, birnessite has a main Raman mode at ~643 cm^{-1},[23-25] and it could be broadened when the interlayer cations are substituted with monolayer species.[18,24] Indeed, as can be seen from Figure 1F, LDH-Bir showed a broadened peak at ~649 cm^{-1}, further confirming the successful cation exchange processes to form LDH-Bir from K-Bir.

The oxidation states of transition metal ions in the as-prepared birnessites were investigated by X-ray photoelectron spectroscopy (XPS, **Figure S6**). Firstly, the binding energy of Mn 2p spin-orbital in K-Bir is much higher than that in LDH-Bir (**Figure 2A**, top panel), indicating a higher oxidation state of the Mn ions in K-Bir. The average oxidation states (AOS) of Mn in these two birnessites were further estimated from the peak splitting of Mn 3s, which represents the exchange interactions of the 3s electrons with the 3d electrons.[26,27] The calculated AOS of Mn in LDH-Bir and K-Bir was 3.10 and 3.93, respectively (**Figure 2A**, bottom panel), further verifying the hybridization induced lowering of the Mn oxidation state, i.e., there were more Mn(III) ions[28] in the LDH-Bir hybrid than in the pristine Bir. As reported, Mn(III) ions take a high spin electron configuration, which would promote fast self-exchange, weaken the Mn-O bonds, and thus promote OER kinetics.[29] Moreover, the robust Mn(IV)O_2 matrix, other than embedding and dispersing the Mn(III) ions, could also help to retain the whole structure and to stabilize the uniformly distributed Mn(III) ions, and thus enhance the stability of the hybrid catalyst even during the OER process (**Scheme 1F**, top panel). ^{1}H solid state nuclear magnetic resonance (^{1}H-ssNMR) spectroscopy was further applied to provide implications about the proton movement on microsecond or faster time scales.[30] The ^{1}H NMR resonances for K-Bir and LDH-Bir (**Figure 2C&2D**) were observed at 7.41 and 6.90 ppm, respectively, indicating a weaker hydrogen bonding and thus a smaller acidity in LDH-Bir.[31] Note that the ratio of LDH/Bir is ~ 1/20 in LDH-Bir, so the NMR signals should be mainly from birnessite. The weak acidity we observed would prohibit the dissolution of catalytic sites[32] and thus make the LDH-birnessite more stable than K-Bir under high current densities in electrocatalytic reactions.

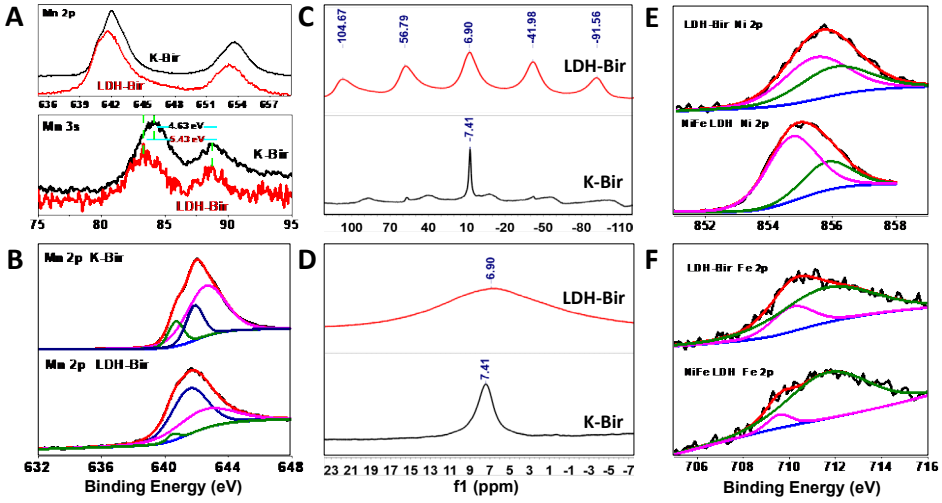

Figure 2. Structure and bonding information of the as-prepared birnessite. (A) The XPS spectra of original K-Bir and LDH-Bir hybrid at (A) Mn 2p and 3s spin-orbitals. (B) The convoluted XPS spectra of LDH-Bir and K-Bir at Mn 2p. (C-D) ^{1}H solid-state NMR (^{1}H-ssNMR) spectra of K-Bir and LDH-Bir. (E-F) The deconvoluted XPS spectra of LDH-Bir and LDH at (E) Ni 2p and (F) Fe 2p.

To identify the reasons behind the oxidation state change of Mn in birnessite upon the intercalation of NiFe LDH, high resolution XPS spectra of the samples in Ni and Fe spin-orbitals were collected and analysed. From the XPS in the Ni 2p

region, it is clear that the peak was positively shifted to 856 eV for LDH-Bir from 855 eV for LDH (**Figure 2E**, **Figure S7**), evidencing more Ni in high oxidation states of LDH-Bir when compared with LDH alone. Since the high oxidation of Ni is widely known to be electrocatalytically active species for OER, the LDH-Bir hybrid would show more advanced performance toward water oxidation than LDH. Meanwhile, it is unexpected to find that Fe in LDH-Bir hybrid showed a decreased oxidation state than that in the LDH from the Fe 2p XPS (**Figure 2F**, **Figure S8**). The deconvoluted spectra further confirmed the lower concentration of Fe in high oxidation states. It is thus reasonable to propose that electron transfer took place between the MnO_2 layer and the LDH layer when they were self-assembled into the LDH(+)-Bir(-) hybrid. This electrostatic 2D nature of the hybrid catalyst would directly impact on the OER process, which will be discussed further below together with the DFT results.

Next, electrochemical performance of the prepared birnessites was evaluated in a typical three-electrode system, by using Pt wire/carbon rod, Hg-HgO and birnessites coated nickel foam (NF) as the counter, reference and working electrode, respectively, if not otherwise indicated (see supporting information, SI for details). Before testing, cyclic voltammetry (CV) curves were collected for more than 100 cycles until a stable CV curve was obtained (**Figure 3A**). From the linear sweep voltammetry (LSV) curves (**Figure 3B**), it can be seen that the overpotential of OER on K-Bir was 362 mV at the current density of 10 mA/cm², which was greatly decreased to 237 mV on LDH-Bir. The overpotential of OER on LDH-Bir was even smaller than that of the prominent catalyst NiFe LDH (258 mV), not to mention birnessite based OER catalysts reported in the literature.[8-10,13,17,21,22,25,33-35] What's more, the overpotential to achieve the current density of 400 mA/cm² was as small as 330 mV for LDH-Bir, suggesting the promising potential applications of this hybrid catalyst for industrial hydrogen production via water splitting. To avoid the possible influence of Pt counter electrode, graphitic rod was applied as the counter electrode. The polarization curves showed negligible change when compared with that using Pt wire as the counter electrode (**Figure S9**). To investigate the steady state reaction kinetics of OER catalysed by the two birnessites, Tafel plots were collected at the scan rate of 1 mV/s. From Figure 3B, the Tafel slope with K-Bir was calculated to be 106 mV/dec (**Figure 3C**, black curve), which was close to the previously reported values.[18,36] However, for OER catalysed by LDH-Bir, the Tafel slope was drastically reduced to 43 mV/dec (**Figure 3C**, red curve), even much lower than that of NiFe LDH (60 mV/dec, **Figure 3C**, purple curve). Indeed, the hybrid catalyst outcompetes the best birnessite based catalyst for OER reported thus far.[7,8,10,13,17,19,21,22,34]

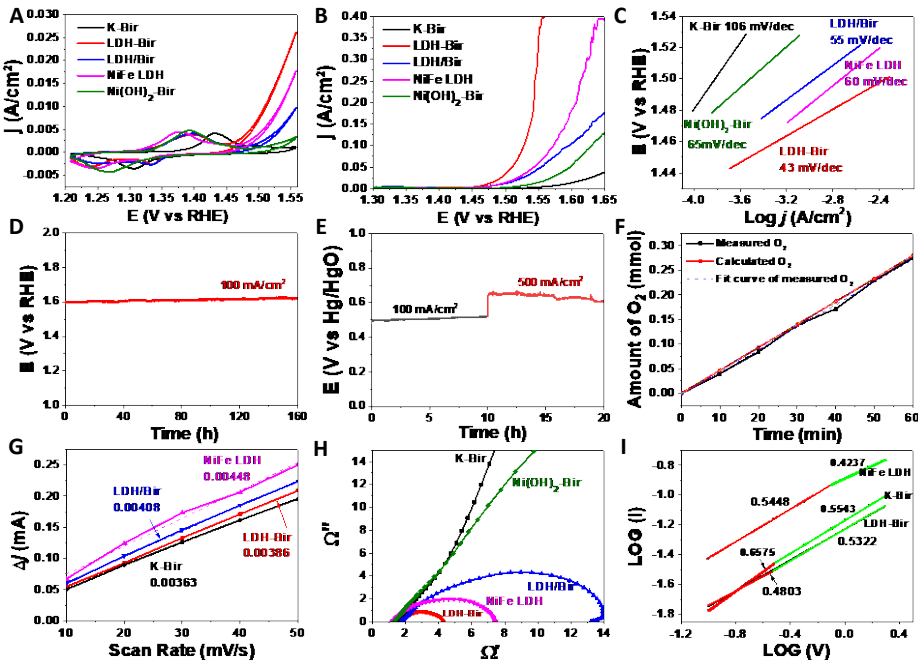

Figure 3. Electrochemical performance characterizations. (A) Stable CV curves after 100 cycles, (B) Linear sweep voltammetry (lsv) polarization curves, (C) Tafel plots, (D) Catalytic stability testing by chronopotentiometry measurement in 1 M KOH and at room temperature, (E) Catalytic stability testing under industry operating conditions of 6 M KOH and 85 °C. (F) Faradaic efficiency evaluation, (G) Double layer capacitance (C_{dl}) measurements, (H) Electrochemical impedance spectra (EIS), and (I) Charge transfer coefficient estimates by using log (I_p, oxidation peak current) *vs* log (v, scan rate) for K-Bir, LDH-Bir, and NiFe LDH.

As mentioned above, the abundant catalytic active Mn(III) centers in the Mn(IV)O_2 matrix of LDH-Bir would be stabilized in the uniformly dispersed state during the OER process (Scheme 1D), promising advanced long-term stability of the novel catalyst. Moreover, the ^{1}H NMR results also suggest that LDH-Bir had a relatively weak hydrogen bonding structure that would be conducive to the stabilization of active sites (**Figure 2C&2D**), making the LDH-Bir a stable electrocatalyst even under high current densities. To confirm the high stability, we performed chronopotentiometry tests. From **Figure 3D**, one can see that the potential for keeping the current density of 100 mA/cm^2 for more than 160 h showed negligible increase, demonstrating the good long-term stability of the LDH-Bir hybrid catalyst than its references (**Figure S10**). Even under the industrial conditions of 85 °C and 6 M KOH, LDH-Bir also exhibited excellent stability. There was only less than 1.5% increase of the potential while holding the high current density of 100 and 500 mA/cm^2 for more than 20 h (**Figure 3E**), further supporting the high operational stability of the prepared LDH-Bir for industrial hydrogen production via water splitting. More encouragingly, the potential for keeping the current density of 500 mA/cm^2 was ~0.64 V (vs Hg/HgO), i.e., ~1.64 V vs RHE, making the 2D-2D hybrid among the most prominent noble-metal free electrocatalysts towards OER under industrial alkaline hydrogen production conditions. Moreover, the Faradaic efficiency (FE) determined by measuring the generated O_2 and H_2 (at the current density of 30 mV/dec for ~1 h (**Figure 3F**) with the consumed electricity was 97%, close to the theoretical FE of 100%. Our results suggest that the advanced catalytic performance of the LDH-Bir mainly originated from the greatly enhanced charge transfer (Figure 3H) and the synergistic effects between the LDH(+) and the birnessite(-) layers, rather than the enhancement of electrochemical surface area **(Figure 3G)** and the modification of reaction mechanism **(Figure 3I)**. This aspect will be discussed in more detail below.

Discussion

To gain a deeper understanding of the activity and stability enhancement of the 2D-2D hybrid catalyst, DFT calculations (**Figure 4**) were carried out. We will present these results below in combination with the experimental findings presented above to clarify several key issues.

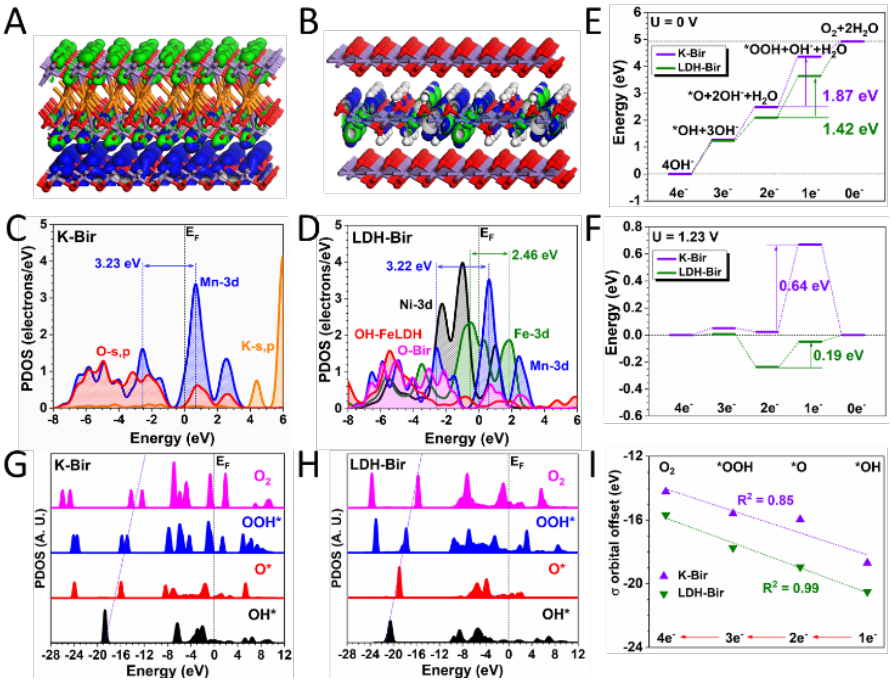

Figure 4. DFT calculations. Bonding and anti-bonding orbital distributions near E_F for (A) K-Bir and (B) LDH-Bir. The PDOS of (C) K-Bir and (D) LDH -Bir. Energy diagram of the OER under (E) U= 0 V and (F) U=1.23 V on K-Bir and LDH-Bir. The PDOS comparison of key adsorbates during OER on (G) K-Bir and (H) LDH-Bir. (I) The linear correlation in electronic structure comparison for both K-Bir and LDH-Bir. The red, purple, orange, blue, light purple and white spheres in (A) and (B) indicate O, Mn, K, Fe, Ni, H, atoms, respectively.

1, Origin of the enhanced catalytic activity of LDH-Bir hybrid catalyst

To explain the greatly improved catalytic performance of LDH-Bir, intrinsic catalytic activity, charge transfer resistance, electrochemical active surface area (ECSA), catalytic mechanism, as well as the interactions between the LDH and MnO_2 layers were further analysed based on experimental and theoretical results. Note that the models for theoretical calculations

were constructed based on the crystal structures of LDH-Bir and K-Bir. After relaxation, the interlayer distance of MnO_2 has been expanded, in which the LDH-Bir hybrid demonstrates a much larger interlayer distance of 7.42 Å (**Figure 4B**) than that of K-Bir (6.66 Å, **Figure 4A**), in accordance with the XRD and HRTEM results.

1.1 Influence of ECSA

Firstly, the ECSA was estimated by the simple CV method (**Figure S11**).[37,38] The calculated double layer capacitance, which is linearly related to ECSA, was close to each other **(Figure 3G)**, in accordance with the similar atomic structure of the two birnessites (SEM, XRD and TEM). This suggests that ECSA, which characterizes the number of active sites, would not be the major factor for the distinctly different OER performance of LDH-Bir and K-Bir toward OER.

1.2 Influence of charge transfer

The charge transfer resistance (R_{CT}) of the as-prepared birnessites was measured. From **Figure 3H**, one can see that the diameter of Nyquist semicircles of LDH-Bir showed a greatly decreased diameter, indicating a much-increased charge transfer rate. Evidently, the facilitated charge transfer benefitted the OER processes on LDH-Bir, in keeping with the above proposed electron transfer between the LDH and MnO_2 layers in LDH-Bir. In order to further identify the causes for the increased charge transfer, the EIS spectra of $Ni(OH)_2$-Bir (without Fe ion in LDH) and the physical mixture of LDH and Birnessite (LDH/Bir) were also collected. From Figure 3H, it is clear that the diameter of Nyquist semicircles increased in the order of LDH-Bir < LDH < LDH/Bir < $Ni(OH)_2$-Bir < K-Bir. This result confirms that LDH and the existence of Fe ions in LDH are critical for the enhanced charger transfer ability of LDH(+)-Bir(-).

Theoretically, the electronic structures, the bonding and anti-bonding orbitals near the Fermi level (E_F) of both the LDH-Bir and K-Bir were investigated, which were found to be significantly different. For K-Bir, the electronic distribution is dominated by the intralayer MnO_2 instead of the inserted K ions, implying limited promotion of the electron transfer by the inserted ions (**Figure 4A**). However, for LDH-Bir, the interlayer NiFe LDH modulated the electronic distribution evidently. More specifically, the bonding and anti-bonding orbitals are dominated by the interlayered NiFe LDH, representing the electroactivity region (**Figure 4B**). This inference is consistent with the EIS result that LDH-Bir showed a much smaller diameter of Nyquist semicircle than K-Bir.

1.3 Influence of reaction mechanism

The charge transfer coefficient (b) expressed in the formula of $I_p=a\nu^b$ was investigated to determine the surface/bulk reaction mechanism, where I_p and ν are oxidation peak current and scan rate of CV curves (**Figure S12**), respectively. As shown in **Figure 3G**, the value of b calculated from the slope of log (I_p) *vs* logν plot was 0.55 for K-Bir and 0.53 for LDH-Bir, respectively, and both were quite close to the value of 0.5, indicating the reaction being diffusion-controlled from either the mass transport within the bulk electrode or the concentration polarization of the electrolyte.[39,40] Therefore, despite the much smaller charge transfer resistance of OER on LDH-Bir, the reaction mechanism and the rate-determining step were proposed to be similar for OER on both K-Bir and LDH-Bir.

Theoretically, the projected partial density of states (PDOSs) is demonstrated to reveal the electronic structure. The insertion of K ions in the interlayer shows the limited influence on the electronic structure of MnO_2, which is attributed to the deep location of *s,p* orbitals of K ions below the E_F, supporting a weak contribution to the OER process (**Figure 4C**). In comparison, in LDH-Bir, the Ni-3d orbitals at the E_V-1.0 eV significantly improve the electroactivity at the interlayered region. The overlapping between Mn-3d, Fe-3d, and Ni-3d orbitals guarantees the site-to-site electron transfer efficiency. The close position of Fe-3d orbitals to the Fermi level exhibit the highly electroactive electron depletion characteristic, which is beneficial for boosting the electron transfer in MnO_2 to enhance the OER performance (**Figure 4D**).

Meanwhile, the OER reaction trend is also revealed to demonstrate the energetic activity owing to the electronic environment modulation. During the calculations, both the reactants and products are considered to reveal the energetic trend. Under the equilibrium potential (U = 0 V), the OER process displays the uphill trend and the largest energy barrier for OER occurs at the reaction of $[O^*+H_2O+2OH^-] \rightarrow [OOH^*+H_2O+OH^-]$ for both LDH-Bir and K-Bir as the rate-determining step (RDS). The RDS barriers for the formation of *OOH are 1.42 eV and 1.87 eV for LDH-Bir and K-Bir, respectively (**Figure 4E**). With the applied standard potential of 1.23 V, the overpotentials of the two structures are estimated. The K-Bir shows an uphill trend until the RDS, demonstrating the overpotential of 0.64 V. In comparison, the initial OER process in LDH-Bir exhibits a nearly spontaneous trend with a much-reduced overpotential of 0.19 V, respectively, which is consistent with the most superior OER performance of LDH-Bir in the experiments (**Figure 4F**). Therefore, the hybridization of LDH into the interlayer of birnessite modifies both the local electronic and energetic activity for the electrocatalysis, which further results in the varied modulation of the OER performances.

1.4 Influence of electronic interactions between the two oppositely charged layers

Experimentally, XPS analysis indicated the electron transfer from Ni to both Mn and Fe, leading to the decreased oxidation states of both. Moreover, to exclude the effect of Fe ions, $Ni(OH)_2$-Bir hybrids were also fabricated and characterized by XPS spectra (**Figure S13**). Here the value of Ni(III)/Ni(II) (**Figure S14**) was greatly reduced to 0.24 ($Ni(OH)_2$-Bir) from 0.74 (LDH-Bir) (**Figure 2E**), indicating a much decreased electron transfer between the $Ni(OH)_2$ monolayer and Bir. Moreover, the ratio of Mn(III)/Mn(IV) (**Figure S15**) was also decreased significantly (from 1.46 for LDH-Bir to 0.91 for $Ni(OH)_2$-Bir), proving the key role of Fe ions in driving the electron transfer to the adjacent MnO_2 layer. This is in accordance with the deteriorated catalytic performance of $Ni(OH)_2$-Bir from LSV curve (**Figure 3B**) and Tafel plots (**Figure 3C**). Therefore, similar to the OEC in PS II where all the metal ions In $CaMn_4O_x$ are catalytically important, the Ni, Mn, and Fe ions with a uniquely modulated electronic structure in the LDH-Bir apparently conspire to work in concert making the 2D-2D hybrid among the most active OER catalysts in this work.

The modified electronic structure also affects the interactions between the catalyst and the intermediates during OER, where the PDOSs of the individual key intermediates have been plotted for the linear correlation level of σ orbitals of *s, p* bands. In comparison, the p-π orbitals only indicate the electroactivity of lattice O. From **Figure 4G**, it is clear that a loss of the linear correlation for the K-Bir is noted, confirming the less efficient electron transfer process for the conversion of O* towards *OOH during the OER. In comparison, for LDH-Bir, the deviation of the σ orbitals is not obvious, which guarantees a high electron transfer efficiency during the OER (**Figure 4H**). The linear correlation of the σ orbitals with the upshifting trend is well preserved, which not only indicates the most efficient electron transfer but also the optimal adsorption strength of intermediates for OER of LDH-Bir. These results are supportive of the much reduced overpotential in LDH-Bir than the K-Bir for the OER.

From the electronic activity perspective, we propose a novel index descriptor for the electrocatalysis process, which is derived based on the linear correlation between the σ orbitals offset of intermediates and electron transfer numbers. The π orbitals of O-species near the Fermi level usually relate to the electroactivity of the lattice O. In comparison, the σ orbitals offset of intermediates demonstrate the electron transfer process, which is affected by the interaction with the catalyst surface. Thus, such a descriptor is able to quantitatively compare the electronic activity of different materials. The linear correlation level is revealed by the linear coefficient R^2, which represents the electron transfer process between the adsorbates and the catalyst. The higher R^2 of the linear fitting indicates efficient electrocatalysis. Different material not only influence the linear coefficient R^2, but also the intercept and the slope. More importantly, the overbinding and non-bonding of intermediates lead to the opposite deviation of σ orbitals offset, which both lower the electron transfer efficiency and hinder the OER process. Such deviations also correlate with the energetic activity regarding the adsorption energies of the intermediates. Notably, LDH-Bir shows a highly linear relationship with $R^2 = 0.99$ after the fitting, where the intercept and slope difference is determined by the nature of the materials. The deviations at the adsorption of *O is noted for K-Bir, resulting in the reduced linear correlation in K-Bir, where the fitting R^2 is 0.85. Therefore, the electronic environment results confirm the different influence level on the layered MnO_2, and the electroactivity of LDH-Bir is much higher than that of K-Bir, supporting the experimental results (**Figure 4I**).

2, Origin of the enhanced stability of the LDH-Bir hybrid catalyst

As mentioned above, the LDH-Bir hybrid catalyst could operate stably at high current densities and under harsh reaction conditions. What is the possible origin for the special stability? First of all, the abundant catalytic active Mn(III) in the $Mn(IV)O_2$ matrix of LDH-Bir would be stabilized in the dispersed state during the OER process (**Scheme 1D**), promising advanced long-term stability of the novel catalyst. Moreover, the enlarged interlayer distance would facilitate the fast electrolyte transport and hence reduce the local proton concentration that would lead to the dissolution of the active site.[32] The weak hydrogen bonding structure of LDH-Bir from the ^1H ssNMR results further confirmed the conducive structure of LDH-Bir hybrid that was beneficial to the stabilization of active sites (**Figure 2C&2D**), making it extremely stable even under high current densities.

From the theoretical calculations, we also investigate the electronic structure of MnO_2. In both K-Bir and LDH-Bir, the insertion of ions barely changes the electronic structure of MnO_2. It is noted, the electronic structure of Mn-3d in K-Bir and LDH-Bir has not been perturbed, where the e_g-t_{2g} splitting maintains highly similar with 3.23 and 3.22 eV, respectively. The O-2p orbitals are also pinned at a similar position. Therefore, the highly stable electronic structure with different ions supports the superior stability of the host structure even with interlayer molecules (**Figure 4C&4D**).

Conclusions

In summary, we designed and constructed an efficient hybrid catalyst toward advanced water oxidation under industrial operating conditions, by intercalating the positively charged NiFe LDH monolayer into the interspace between the negatively charged birnessite layers. The as-prepared 2D-2D LDH(+)-Bir(-) hybrid catalyst showed excellent activity in alkaline solutions with a very low overpotential of 330 mV at a very high current density (400 mA/cm^2) and small Tafel slope

of 43 mV/dec, and promising long-term stability even under the industrial hydrogen production conditions of 85 °C and 6 M KOH. There was only less than 2% increase in potential while keeping the current density of 500 mA/cm² at 0.64 V (vs Hg/HgO) for more than 10 h. From both the experimental and theoretical results, electron transfer between the two oppositely charged 2D layers occured, which together with the interlayer electric field contributes to the largely enhanced reaction kinetics of OER. Moreover, the intercalation of LDH monolayer into the interlayer of birnessite also optimized the absorbing-desorbing properties of this hybrid catalyst, leading to both the efficient and the stable OER performance. Through such a novel 2D-2D electrostatic assembly strategy, the flexible modulation of electrocatalyst is realized, which opens a unique approach for designing efficient clean fuel transforming electrocatalysts.

ASSOCIATED CONTENT

Supporting Information. SEM and TEM images, XPS spectra, electrochemical tests are included. "This material is available free of charge via the Internet at http://pubs.acs.org."

AUTHOR INFORMATION

Corresponding Author

*Corresponding author: xialong@pku.edu.cn, bhuang@polyu.edu.hk, chsyang@pku.edu.cn

Author Contributions

All authors have given approval to the final version of the manuscript. / ‡These authors contributed equally.

Funding Sources

This work was financially supported by National Natural Science Foundation of China (21703003, 21972006, 21771156), Shenzhen Peacock Plan (KQTD20160530155440 57), Shenzhen Science and Technology Innovation Commission (JCYJ20180302153417057, JCYJ20190808155413194), Nanshan Pilot Plan (LHTD20170001), and the Early Career Scheme (ECS) fund (PolyU 253026/16P) from the Research Grant Council (RGC) in Hong Kong.

Notes

The authors declare no competing financial interest.

REFERENCES

(1) Ju, M.; Wang, X. T.; Long, X.; Yang, S. H. *Crystengcomm* **2020**, *22*, 1531.
(2) Long, X.; Qiu, W.; Wang, Z.; Wang, Y.; Yang, S. H. *Mater. Today Chem.* **2019**, *11*, 16.
(3) Long, X.; Xiao, S.; Wang, Z. L.; Zheng, X. L.; Yang, S. H. *Chem. Commun.* **2015**, *51*, 1120.
(4) Gao, X. Y.; Long, X.; Yu, H.; Pan, X. Y.; Yi, Z. G. *J. Electrochem. Soc.* **2017**, *164*, H307.
(5) Long, X.; Li, J. K.; Xiao, S.; Yan, K. Y.; Wang, Z. L.; Chen, H. N.; Yang, S. H. *Angew. Chem. Int. Edit.* **2014**, *53*, 7584.
(6) Umena, Y.; Kawakami, K.; Shen, J. R.; Kamiya, N. *Nature* **2011**, *473*, 55.
(7) Pinaud, B. A.; Chen, Z.; Abram, D. N.; Jaramillo, T. F. *J. Phys. Chem. C* **2011**, *115*, 11830.
(8) Frey, C. E.; Wiechen, M.; Kurz, P. *Dalton T.* **2014**, *43*, 4370.
(9) Yin, H.; Li, H.; Wang, Y.; Ginder-Vogel, M.; Qiu, G.; Feng, X.; Zheng, L.; Liu, F. *Chem. Geol.* **2014**, *381*, 10.
(10) Wiechen, M.; Najafpour, M. M.; Allakhverdiev, S. I.; Spiccia, L. *Energ. Environ. Sci.* **2014**, *7*, 2203.
(11) McKendry, I. G.; Kondaveeti, S. K.; Shumlas, S. L.; Strongin, D. R.; Zdilla, M. J. *Dalton T.* **2015**, *44*, 12981.
(12) Lucht, K. P.; Mendoza-Cortes, J. L. *J. Phys. Chem. C* **2015**, *119*, 22838.
(13) Takashima, T.; Hashimoto, K.; Nakamura, R. *J. Am. Chem. Soc.* **2012**, *134*, 1519.
(14) Robinson, D. M.; Go, Y. B.; Mui, M.; Gardner, G.; Zhang, Z.; Mastrogiovanni, D.; Garfunkel, E.; Li, J.; Greenblatt, M.; Dismukes, G. C. *J. Am. Chem. Soc.* **2013**, *135*, 3494.
(15) Peng, H.; McKendry, I. G.; Ding, R.; Thenuwara, A. C.; Kang, Q.; Shumlas, S. L.; Strongin, D. R.; Zdilla, M. J.; Perdew, J. P. *P. Natl. Acad. Sci. USA* **2017**, *114*, 9523.
(16) Maitra, U.; Naidu, B. S.; Govindaraj, A.; Rao, C. N. R. *P. Natl. Acad. Sci. USA* **2013**, *110*, 11704.
(17) Thenuwara, A. C.; Cerkez, E. B.; Shumlas, S. L.; Attanayake, N. H.; McKendry, I. G.; Frazer, L.; Borguet, E.; Kang, Q.; Remsing, R. C.; Klein, M. L.; Zdilla, M. J.; Strongin, D. R. *Angew. Chem. Int. Edit.* **2016**, *55*, 10381.
(18) Thenuwara, A. C.; Shumlas, S. L.; Attanayake, N. H.; Cerkez, E. B.; McKendry, I. G.; Frazer, L.; Borguet, E.; Kang, Q.; Zdilla, M. J.; Sun, J.; Strongin, D. R. *Langmuir* **2015**, *31*, 12807.
(19) Thenuwara, A. C.; Shumlas, S. L.; Attanayake, N. H.; Aulin, Y. V.; McKendry, I. G.; Qiao, Q.; Zhu, Y.; Borguet, E.; Zdilla, M. J.; Strongin, D. R. *ACS Catal.* **2016**, *6*, 7739.
(20) Birkner, N.; Nayeri, S.; Pashaei, B.; Najafpour, M. M.; Casey, W. H.; Navrotsky, A. *P. Natl. Acad. Sci. USA* **2013**, *110*, 8801.
(21) Wiechen, M.; Zaharieva, I.; Dau, H.; Kurz, P. *Chem. Sci.* **2012**, *3*, 2330.
(22) Chen, Z.; Wang, Z.; Cai, R.; Xie, Y.; Yu, J.; Long, X.; Yang, B.; Yang, S. *Nanoscale* **2020**.
(23) Chen, D.; Ding, D.; Li, X.; Waller, G. H.; Xiong, X.; El-Sayed, M. A.; Liu, M. *Chem. Mater.* **2015**, *27*, 6608.
(24) Julien, C.; Massot, M.; Baddour-Hadjean, R.; Franger, S.; Bach, S.; Pereira-Ramos, J. P. *Solid State Ionics* **2003**, *159*, 345.
(25) Hsu, Y.-K.; Chen, Y.-C.; Lin, Y.-G.; Chen, L.-C.; Chen, K.-H. *Chem. Comm.* **2011**, *47*, 1252.
(26) Rao, C. N. R.; Sarma, D. D.; Vasudevan, S.; Hegde, M. S.; Thomas, J. M. *P. Roy. Soc. A-Math. Phy.* **1979**, *367*, 239.
(27) Galakhov, V. R.; Demeter, M.; Bartkowski, S.; Neumann, M.; Ovechkina, N. A.; Kurmaev, E. Z.; Lobachevskaya, N. I.; Mukovskii, Y. M.; Mitchell, J.; Ederer, D. L. *Phys. Rev. B: Condens. Matter Mater. Phys.* **2002**, *65*, 11302.
(28) Huynh, M.; Shi, C.; Billinge, S. J. L.; Nocera, D. G. *J. Am. Chem. Soc.* **2015**, *137*, 14887.
(29) Huynh, M.; Bediako, D. K.; Nocera, D. G. *J. Am. Chem. Soc.* **2014**, *136*, 6002.
(30) Mitchell, J. B.; Geise, N. R.; Paterson, A. R.; Osti, N. C.; Sun, Y.; Fleischmann, S.; Zhang, R.; Madsen, L. A.; Toney, M. F.; Jiang, D.-e.; Kolesnikov, A. I.; Mamontov, E.; Augustyn, V. *ACS Energy Lett.* **2019**, *4*, 2805.
(31) Sideris, P. J.; Nielsen, U. G.; Gan, Z.; Grey, C. P. *Science* **2008**, *321*, 113.

(32) Chen, R.; Hung, S. F.; Zhou, D. J.; Gao, J. J.; Yang, C. J.; Tao, H. B.; Yang, H. B.; Zhang, L. P.; Zhang, L. L.; Xiong, Q. H.; Chen, H. M.; Liu, B. *Adv. Mater.* **2019**, *31*.
(33) Birkner, N.; Nayeri, S.; Pashaei, B.; Najafpour, M. M.; Casey, W. H.; Navrotsky, A. *Proc. Natl. Acad. Sci. USA* **2013**, *110*, 8801.
(34) McKendry, I. G.; Thenuwara, A. C.; Shumlas, S. L.; Peng, H.; Aulin, Y. V.; Chinnam, P. R.; Borguet, E.; Strongin, D. R.; Zdilla, M. J. *Inorg. Chem.* **2018**, *57*, 557.
(35) Frey, C. E.; Wiechen, M.; Kurz, P. *Dalton T.* **2014**, *43*, 4370.
(36) Li, N.; Hu, Z.; Li, M.; Zhang, L.; Hu, S. *Mater. Lett.* **2020**, *281*, 128569.
(37) Xie, Y.-S.; Wang, Z.; Ju, M.; Long, X.; Yang, S. *Chem. Sci.* **2019**, *10*, 8354.
(38) Gao, X.; Pan, X.; Long, X.; Yi, Z. *J. Electrochem. Soc.* **2017**, *164*, H755.
(39) Brezesinski, T.; Wang, J.; Polleux, J.; Dunn, B.; Tolbert, S. H. *J. Am. Chem. Soc.* **2009**, *131*, 1802.
(40) Lyons, M. E. G.; Brandon, M. P. *Phys. Chem. Chem. Phys.* **2009**, *11*, 2203.

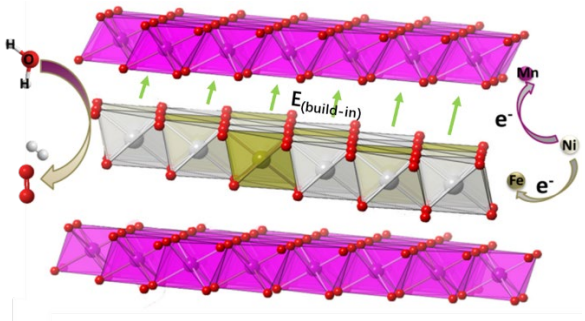
H
O
H
$E_{(build-in)}$
Mn
e-
Ni
Fe
e-